Two Stage to Orbit Using a Hypersonic First Stage and Horizontal Launch

Mr. Michael Paluszek[*,a]**, Dr. Christopher Galea**[a]**, and Ms. Stephanie Thomas**[a]

[a]*Princeton Satellite Systems, Plainsboro, NJ*
[*]Corresponding author

ABSTRACT

With the expansion of space commercialization, the need for rapid access to space is increasing. To date, all operational launch vehicles have been vertical launches. Some are reducing costs by recovering and reusing their first stages. Recovery of payloads from orbit is performed using capsules, the same technology that has been used since the Vostok. Space planes, such as the US X-37B and the Chinese space plane are in operation but they are launched by rockets.

This paper expands on the authors' past work on the Space Rapid Transit vehicle, a two-stage to-orbit vehicle that takes off horizontally and lands horizontally. The vehicle is sized to carry 500 kg to an ISS orbit and is fully reusable. The first stage is powered by a hydrogen-fueled RDE ramjet with a subsonic rotating detonation combustor. The second stage uses liquid hydrogen and liquid oxygen propellants. The stages separate using their reaction control systems.

The new results in this paper cover the control of the two vehicles in the atmosphere and the optimization of the separation Mach number and altitude. The control system transitions from all aerodynamic to mixed reaction and aerodynamic control. The control is partitioned into torque and force demand and actuator (thruster or aerodynamic) and force and torque distribution. This results in a very robust controller. Nonlinear plant inversion is used to implement the core trajectory controller. Control during separation is discussed. An event-based trajectory optimization algorithm is presented. The optimizer selects set points that are implemented by the control system.

The resulting two-stage vehicle is demonstrated in numerical simulations. The simulations go from takeoff roll to orbit. The trajectory for the rocket second stage is presented. Future work is discussed.

1. INTRODUCTION

Hypersonic aircraft and missiles are of great interest. Potential applications include military reconnaissance and strike, passenger aircraft, and the first stage for a two-stage to-orbit launch vehicle [1, 2, 3, 4, 5]. Numerous engines have been proposed for hypersonic vehicles including a wide variety of combined cycle engines, such as those with integrated rockets and scramjets. Engines that have been tested or are currently under test include the Sänger II turboramjet [6] and the Reaction Engines Limited [7] cooled inlet engine.

Space planes, including the X-37B and the Chinese Reusable Experimental Spacecraft 可重使用航天器 (CSSHQ) [8], are in operation. The X-37B was recently launched on a Falcon 9 Heavy [9] and the Chinese plane launched for the third time in December, 2023 [10]. Sierra Space's Dream Chaser is expected to make its first launch to the ISS this year [11]. None of these can reach orbit without additional stages. They all are reusable and land at airfields. There is some discussion of China using a scramjet-powered first stage in future vehicles [12].

Figure 1: Sierra Space's Dream Chaser space plane at NASA's Neil Armstrong Test Facility. (Image credit: Future/Josh Dinner)

Our specific application is an engine for a two-stage to-orbit launch vehicle. The first stage takes off from an airfield and accelerates to a high Mach number and then the second stage separates. The second stage uses an LH_2/LO_2 engine, such as the Aerojet Rocketdyne's RL-10 to take the spacecraft into orbit and return the second stage to the airfield. The first stage returns to the launch site at subsonic speeds. The first stage engine is the subject of this paper. The entire two-stage to-orbit vehicle is discussed in detail in [1].

The turbojet allows operation up to Mach 1.25 and is capable of accelerating through Mach 1. An important point to note is that the ramjet is only used as an accelerator. This greatly decreases the stress on the engine compared to one that must operate for hours at high Mach cruise speeds. Coaxial ramjets are not new. The J58 engine in the SR-71 was a coaxial ramjet designed to cruise at Mach 3.2. The coaxial ramjet is the same concept that was proposed for the Sänger two-stage to-orbit vehicle [13]. That engine is shown in the test in Figure 2.
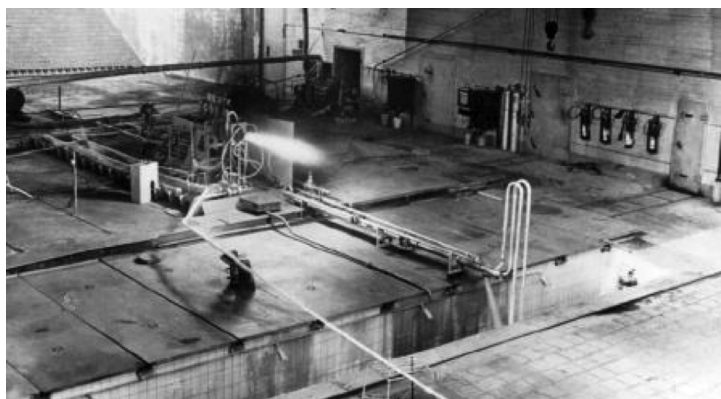

Figure 2: The hydrogen-fueled MBB Turboramjet in test [14]. The Sänger first stage would have cruised at Mach 4 and accelerated to Mach 6.8 before second stage separation. The large vehicle was capable of launching geosynchronous communications satellites.

Work is underway at other companies on hypersonic air-breathing engines. GE has a hypersonic engine with an RDE combustor in test [15, 16]. The Hermeus Corporation is beginning the test of a turboramjet [17]. Hermeus uses a Pratt & Whitney F100 engine as the core.

The paper starts by reviewing the concept of operations in Section 2. An engine with a Rotating Detonation Engine is discussed in Section 3 with a combustor. The section presents a simulation from takeoff to orbit for both a turboramjet and an RDE-based engine. Section 4 describes an event-based trajectory optimization using a delta-v velocity map for the second stage and an analytical engine stress model for the first stage engine is given in Section 5. The first stage trajectory optimization is a weighted combination of engine stress and terminal Mach number and altitude and is presented in Section 8. The control systems are discussed in Section 6.

2. Launch Concept of Operations

Space Rapid Transit (SRT), Figure 3 is a horizontal-takeoff launch vehicle concept that would revolutionize both the space launch and flight transportation industries. To break the cycle of escalating space launch systems costs, it is necessary to consider concepts that are drastically different from current launch options. The full system, Ferry first stage with reusable Orbiter second stage, is expected to cost less than $300/kg to low earth orbit. SRT offers an incremental test platform capable of maturing the technology required for affordable, routine space access and global reach aircraft. The horizontal-takeoff design ensures successful rapid launch, recovery, and refurbishment of the vehicle.

Figure 3: The SRT concept would solve the problem of high launch costs with a production cost of $131/lb to LEO. Background image courtesy of the U.S. Air Force.

The SRT design uses hydrogen fuel which has a much higher specific impulse at altitude than kerosene or jet fuel thus lowering the ratio of vehicle to payload mass. SRT can produce much more velocity change in the first stage than can other airborne launch concepts and has the potential, with turbo ramjets or scramjets, to produce a significant fraction of the total required velocity change to achieve orbit, thus further reducing the system mass. Even the best rockets have an order of magnitude lower specific impulse than air-breathing engines. Note that scramjets, a form of air-breathing engine, at high Mach number have only two to three times higher specific impulse than rockets.

Since SRT is launched from an airfield, specialized launch facilities are not required. SRT does not use hydrazine for either stage and uses linear electric actuation throughout, eliminating the special handling of toxic propellant and hydraulic fluid. The composite thermal protection system also requires minimal maintenance. Flight operations are another cost driver. SRT is designed to be fully autonomous with only two crew on the ground to monitor and override the autonomous systems as needed. Ground operations are shown in Figure 4. Permanent H_2 and O_2 are not required. Standard cranes can handle mating.

SRT would be far safer than vertical launch. Aborts do not require the destruction of the vehicle. If an abort happens when the rocket is operating it can be shut down and the vehicle flown back to its launch site or any compatible landing site. SRT is an aircraft launch system that employs both horizontal takeoff and horizontal landing. SRT has been discussed at length in several papers [2, 3, 4, 5]. SRT is similar in concept to the NASA Beta launch vehicle [18] and the Messerschmitt-Bölkow-Blohm (MBB) Sänger [6].
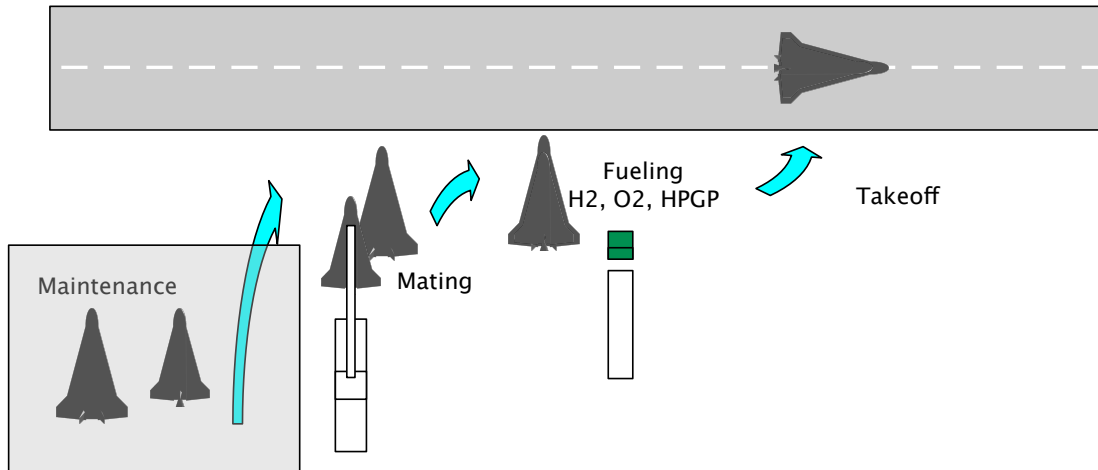
Figure 4: Ground operations. No specialized equipment is required.

The NASA Beta program was a series of conceptual studies between 1986 and 1992 for horizontal takeoff-horizontal landing launch operations. The first vehicle was a 900,000 kg Gross Lift-Off Weight (GLOW) Space Shuttle replacement capable of delivering 22,500 kg to LEO. This was followed by a 450,000 kg GLOW capable of delivering 11,250 kg to LEO. The GLOW for the Space Shuttle was 2,000,000 kg.

Sänger II would place a payload of either two crews and 3,000 kg using the Horus winged upper stage or a 15,000 kg payload with the unmanned Cargus upper stage. The first stage would cruise on turboramjets at Mach 4.4 to the launch area, then dash to Mach 6.5 and release the upper stage. A fully integrated ramjet combustor and H_2 turbine were tested by MBB at Ottobrun [6].

Alternative approaches are fully reusable single-stage horizontal takeoff and landing to orbit such as the Skylon [19, 7]. Horizontal takeoff with expendable upper stages include Pegasus [20], which is in operation and Virgin Galactic's LauncherOne [21]. Each approach has advantages and disadvantages. Single stage to orbit is operationally the simplest but the vehicle must carry the air-breathing engines to orbit, reducing payload. Two stages to orbit require the mating of two vehicles which adds complexity to the ground operations. This is not a major issue for small launch vehicles though large vehicles would need dedicated mating facilities. Horizontal launch vehicles with throwaway upper-stage boosters discard their upper stages. The upper stage cost must be charged to the payloads on the mission. If the launch rate is low, this approach may be the most cost-effective because the more expensive reusable upper-stage manufacturing cost is spread over too few missions to make it economical. Our approach with SRT provides the payload benefits of a two-stage vehicle and a high launch rate to amortize costs for both reusable stages.

3. Rotating Detonation Engine

3.1 Overview

An RDE is an air-breathing aircraft engine that uses a detonation (rather than deflagration) to add energy to the working fluid [22, 23]. Deflagration is the process of heating a material until it burns away. While the flames from deflagration travel at subsonic speeds, the flames from detonation form a shock wave traveling at supersonic speeds. The first detonation sets up a cycle in which the flow circulates the chamber. The pressure from each detonation continues the cycle and forces the exhaust out of the chamber. A compressor is not required but makes the engine more efficient. Unlike a Pulse Detonation Engine, the process is continuous. No chamber purging is required. With detonation, the fuel burns instantaneously, not allowing time for expansion, and this constant volume process can allow higher work output, leading to higher efficiency. A schematic and an annular engine is shown in Figure 5. Annular engines have higher losses than cylindrical engines. However, they are easier to operate. Problems with RDEs include multiple detonations and detonations that cause a reversal of the flow.
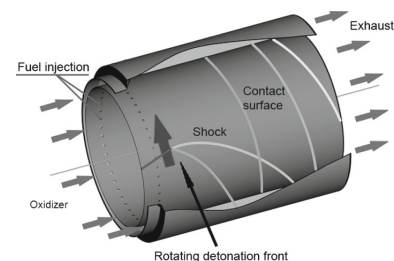

Figure 5: RDE schematic. [22].

The RDE has the potential to improve combustor efficiency. Recent work on RDEs includes an in-space flight test [24, 25] as well as laboratory experimental and computational studies [26, 27]. It may be possible to reach
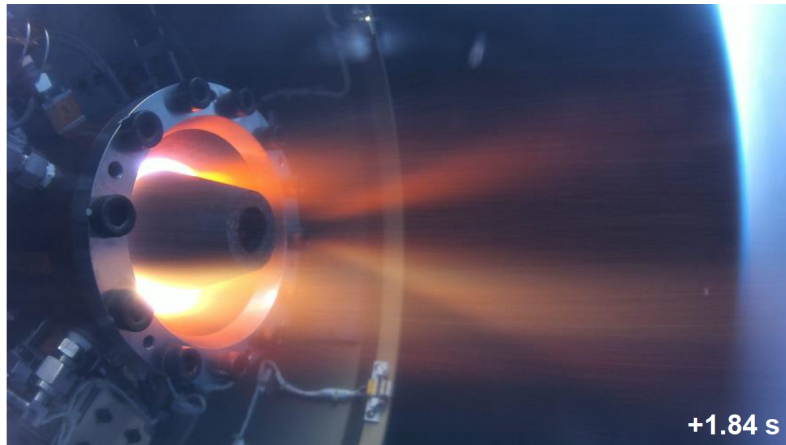
Mach numbers above 6.8, the number planned for the Sänger.

Figure 6: Photo of an RDE test in space, where the high-temperature RDE gas plume is shown. Image from Goto et al. (2022) [24].

GE demonstrated [15, 16] a subscale version of their RDE hypersonic engine [28]. Their work indicates the potential of this concept. The subscale demonstration at the GE Global Research Center is a TBCC system composed of a high-Mach variant of a Mach 2.5-class turbofan paired with a rotating detonation-dual-mode ramjet. The engine transitions from ramjet to scramjet [15].

3.2 Analytical RDE Model

Details of the RDE analytical model can be found in [29]. Figure 7 gives specific thrust and specific impulse as a function of altitude based on the RDE analytical model. The computations use the Shock and Detonation Toolbox [30] and Cantera [31].
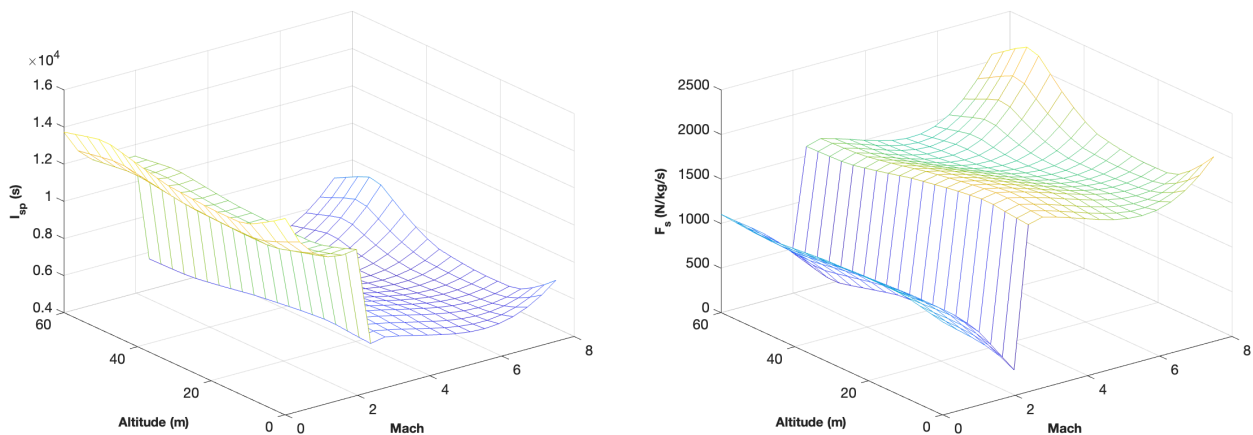

Figure 7: RDE engine maps showing specific impulse, I_{sp}, and specific thrust, F_s.

Figure 8 gives the thrust for a 1 m^2 inlet area and the mode. Mode 0 is for turbojet mode while mode 1 is for RDE mode. The transition to ram pressure is at Mach 2. As might be expected, the thrust drops with altitude for a fixed inlet area since the air mass flow drops with density.

Figure 9 compares the turboramjet with the RDE for one Mach number and altitude profile. The inflection point for the turboramjet is when it switches from turbojet to ramjet. This point can be adjusted for improved performance. However, as the figure shows, the RDE is superior throughout the trajectory. Figure 10 shows the turboramjet engine maps for comparison.

4. Second Stage Trajectory Mapping

The Orbiter takes the payload from separation to LEO. The separation Mach number and altitude would depend on the trajectory of the Ferry. Rather than including the Orbiter trajectory optimization with the Ferry optimization, its trajectories to LEO are mapped using a range of Mach numbers and altitudes. This can be accessed by the optimization through interpolation of the two-dimensional table in the optimization function. The
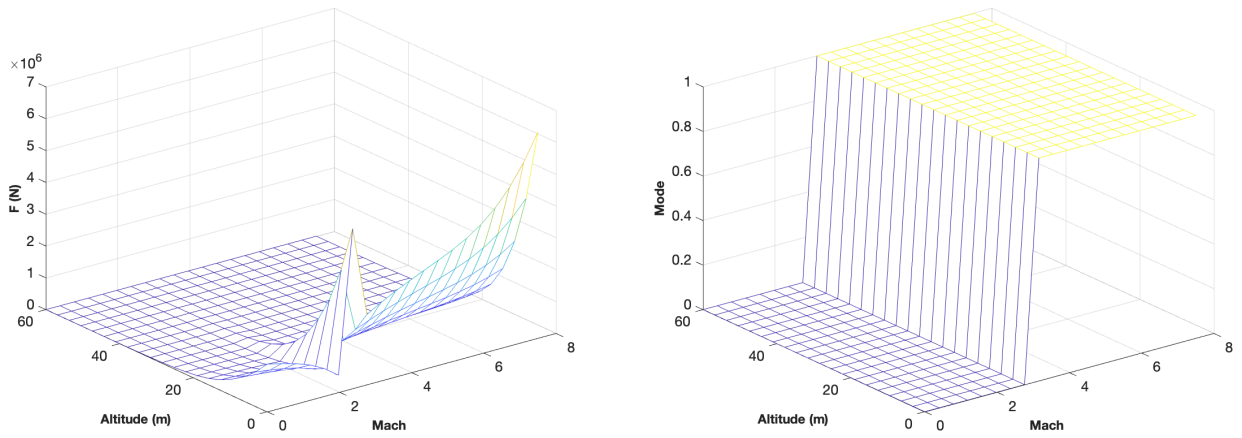
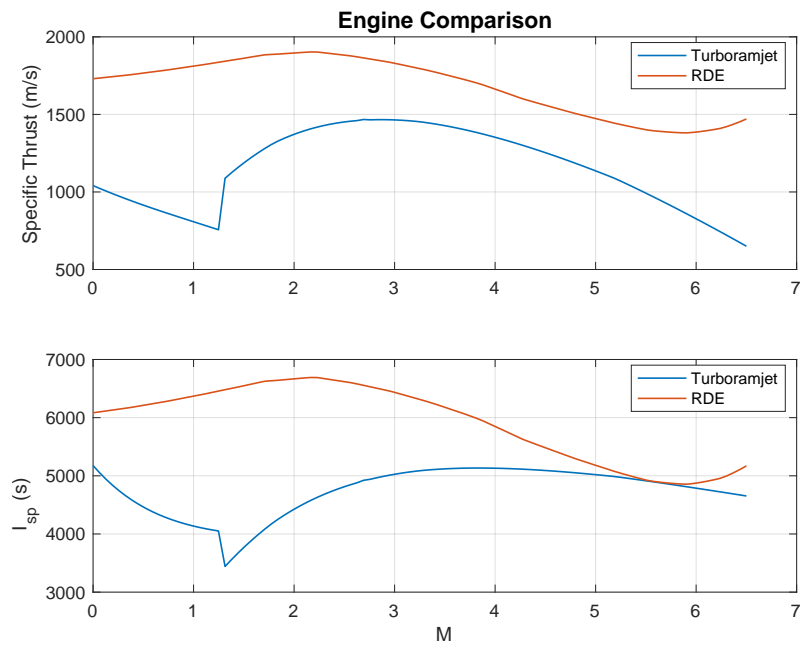**Figure 8:** RDE engine maps show thrust F and mode.

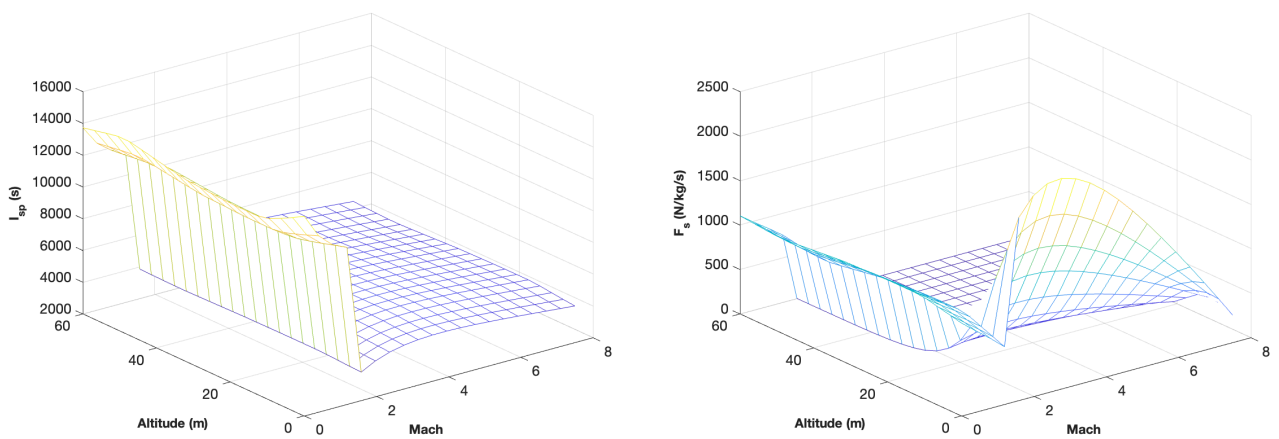**Figure 9:** RDE comparison with a turboramjet.

Figure 10: Turboramjet engine maps showing I_{sp} and F_s.

boost phase consists of the initial insertion burn which puts the Orbiter into a coast arc and the circularization burn which puts it into the drift orbit. Both are done by the H_2/O_2 main engine. The engine has a two-axis gimbal for pitch and yaw control. Roll control is accomplished with the aerodynamic effectors and with the RCS system.

The boost phase begins at altitude h_0, velocity V_0, and flight path angle γ_0. It consists of two burns separated by a coasting period. The first burn brings the SRT Orbiter up out of the atmosphere, placing it on a transfer trajectory with an apogee equal to the target altitude. The second burn circularizes the orbit at altitude h_F with the circular orbit velocity $V_F = \sqrt{\mu/(R_E + h_F)}$ and at $\gamma_F = 0$. Let the initial velocity and flight path angle of the transfer trajectory be denoted as V_{T1} and γ_{T1}, respectively. Similarly, the final velocity and flight path angle of the transfer trajectory are V_{T2} and γ_{T2}, respectively. We assume that the first burn is directed along the initial flight path angle so that $\gamma_{T1} = \gamma_0$. In addition, the transfer is designed so that it reaches its apogee at h_F, meaning that $\gamma_{T2} = \gamma_F = 0$. Thus, the first and second delta-v's are:

$$\Delta V_1 = V_{T1} - V_0 \tag{1}$$
$$\Delta V_2 = V_F - V_{T2} \tag{2}$$

It is possible to derive an expression for the initial and final velocities of the transfer trajectory as a function of the initial flight path angle. We first recognize the following relationships governing the transfer trajectory:

$$H = (R_E + h_0)V_{T1}\cos\gamma_0 \tag{3}$$
$$e^2 = \left(V_{T1}^2 \cos^2\gamma_0 \left(\frac{R_E + h_0}{\mu}\right) - 1\right)^2 + \left(V_{T1}^2 \cos\gamma_0 \sin\gamma_0 \left(\frac{R_E + h_0}{\mu}\right)\right)^2 \tag{4}$$
$$a = \frac{H^2}{\mu(1 - e^2)} \tag{5}$$
$$V_{T2}^2 = \mu\left(\frac{2}{R_E + h_F} - \frac{1}{a}\right) \tag{6}$$

The requirement that the apogee of the transfer trajectory occur at the target orbit altitude gives the additional equation:

$$h_F + R_E = a(1 + e) = \frac{H^2}{\mu(1 - e)} \tag{7}$$

Combining Eq. 3 and Eq. 4 into Eq. 7 and simplifying yields the following expression for the initial transfer velocity:

$$V_{T1}^2 = \left(\frac{2\mu}{R_E + h_0}\right)\left(\frac{1 - f}{1 - f^2 \cos^2\gamma_0}\right) \tag{8}$$

where $f < 1$ is the fraction:

$$f = \frac{R_E + h_0}{R_E + h_F}$$

Thus the total delta-v can be expressed as a function of the initial flight path angle of the boost phase, which is also the terminal flight path angle of the Ferry.

The analysis thus far has neglected drag. We approximate the delta-v required to overcome drag by first computing the drag acceleration history across altitude and then integrating that acceleration history over time. The drag acceleration is given as:

$$a_D(h) = \frac{1}{2}\rho(h)V^2(h)SC_D/m \tag{9}$$

where ρ is the atmospheric density, $S = 4$ m^2 is the reference area, $C_D = 0.05$ is the drag coefficient, and $m = 2,000$ kg is the initial mass of the vehicle. Neglecting mass flow rate and using the initial mass is a sufficient approximation because drag drops off quickly as the altitude increases. The velocity as a function of altitude is found by using Eq. 6 with intermediate altitudes h in place of h_F. The results of this analysis are illustrated in Figure 11 and Figure 12 without drag.

The drag is small. A typical trajectory and drag loss is shown in Figure 13. The atmospheric density model using scale heights is shown.

There is an effect of atmospheric pressure on the Orbiter engine's specific impulse. This is shown in Figure 14. Once the separation altitude becomes greater than 40 km, this effect is small.
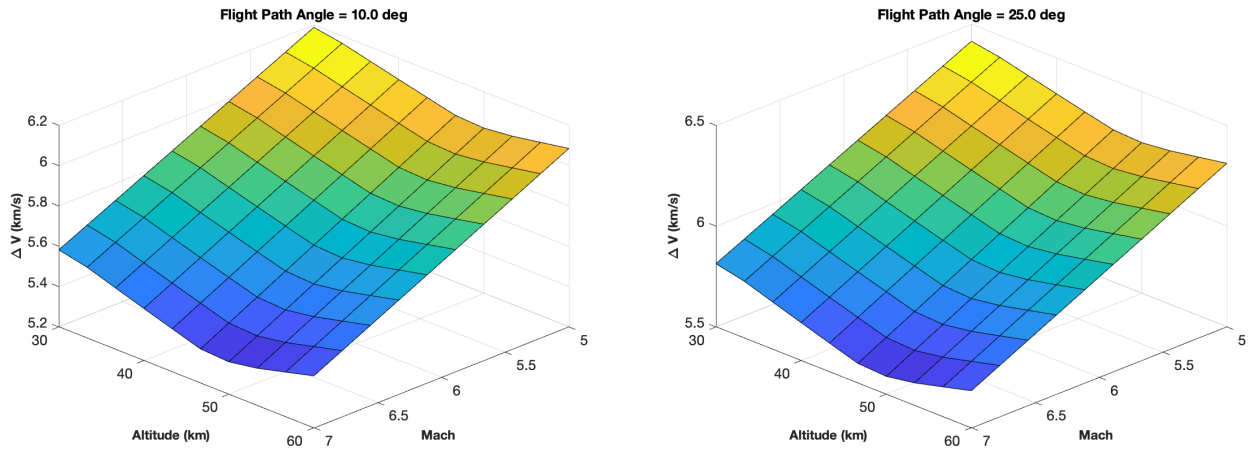
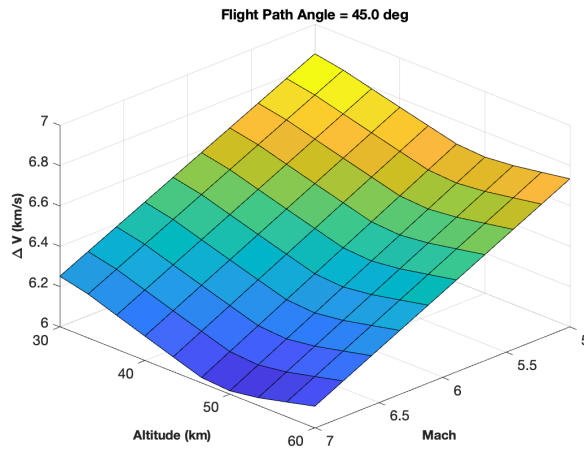**Figure 11:** Delta-V Analysis for the Orbiter with $\gamma_0 = 10$ deg and 25 deg.

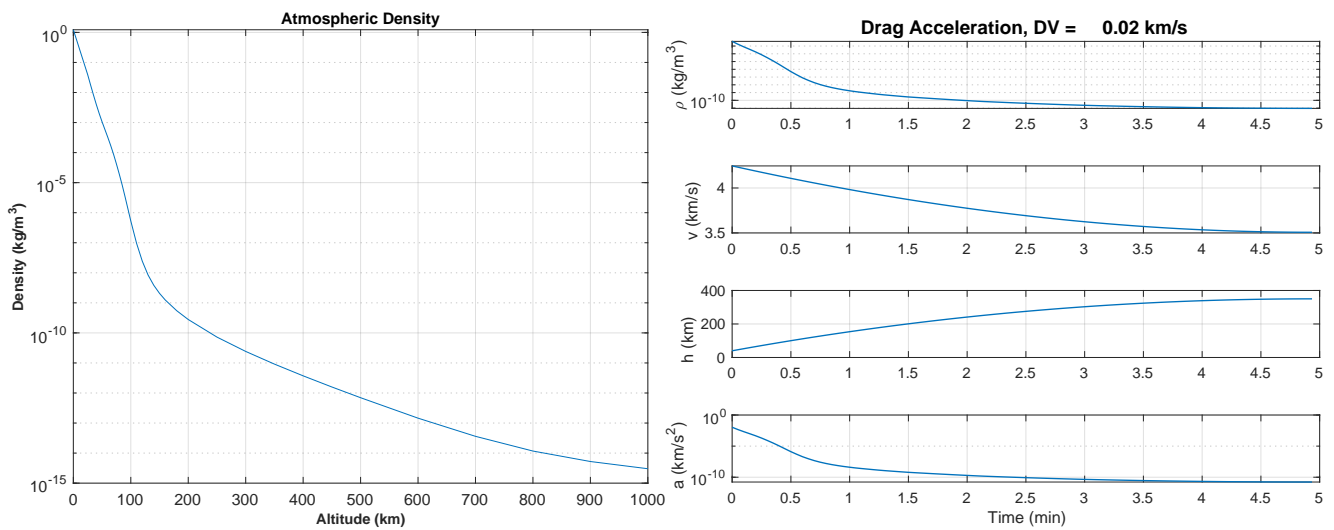**Figure 12:** Delta-V Analysis for the Orbiter with $\gamma_0 = 45$ deg.

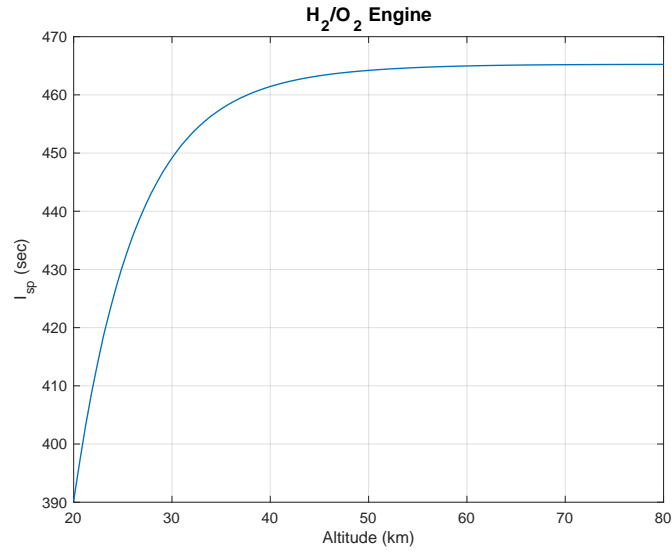**Figure 13:** Drag analysis for a typical Orbiter trajectory.

Figure 14: Effective of altitude on an H_2/O_2 engine.

5. Engine and Inlet Model for Optimization

The engine stress model is based on [32]. The heat flux is

$$\dot{q}_w = \frac{1}{2} c_F p_d v \tag{10}$$

$$c_F = \frac{0.0296}{r_E^{\frac{1}{5}}} \tag{11}$$

$$r_E = \frac{vl}{\mu} \tag{12}$$

$$p_d = \frac{1}{2} \rho v^2 \tag{13}$$

$$v = Ma \tag{14}$$

where μ is the kinematic viscosity, l is the characteristic length, M is Mach number, a is the speed of sound and ρ is the atmospheric density. Typical results are shown in Figure 15.
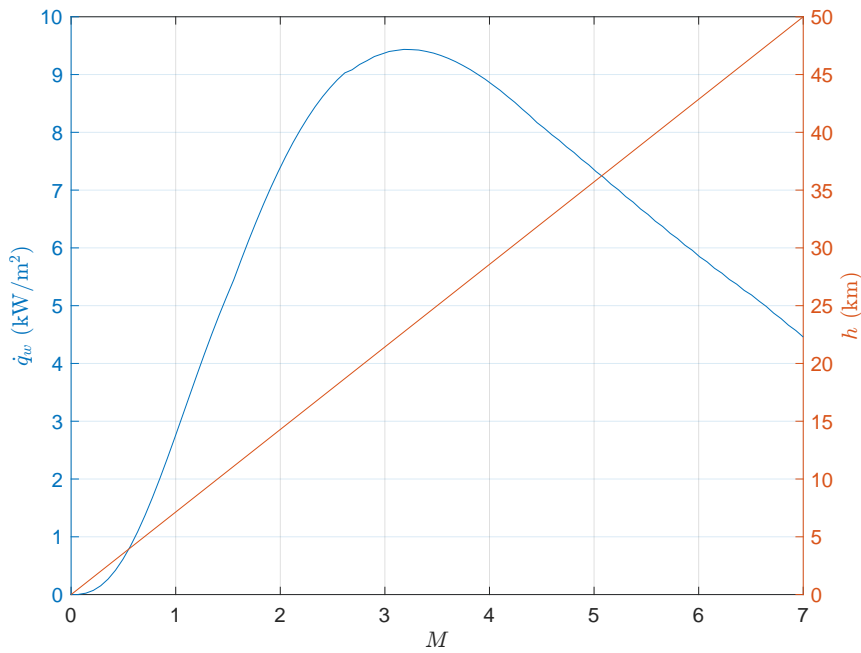

Figure 15: Heat flux as a function of Mach number and altitude.

In this plot, the maximum heat flux is at Mach 3. By adjusting the acceleration we can move this peak.

6. Control

6.1 Overview

The two vehicles, the Ferry and Orbiter, have independent control systems. The Orbiter operates after separation. The Ferry control system is a high-speed aircraft control system. It operates in all flight regimes from takeoff through separation and back to landing. It is fully autonomous but allows operators on the ground to override the automatic systems. The unified control system is shown in Figure 16. Both vehicles fly the same flight software and either vehicle can control the other providing an additional level of redundancy. Further details of the control system can be found in [1, 2, 4].
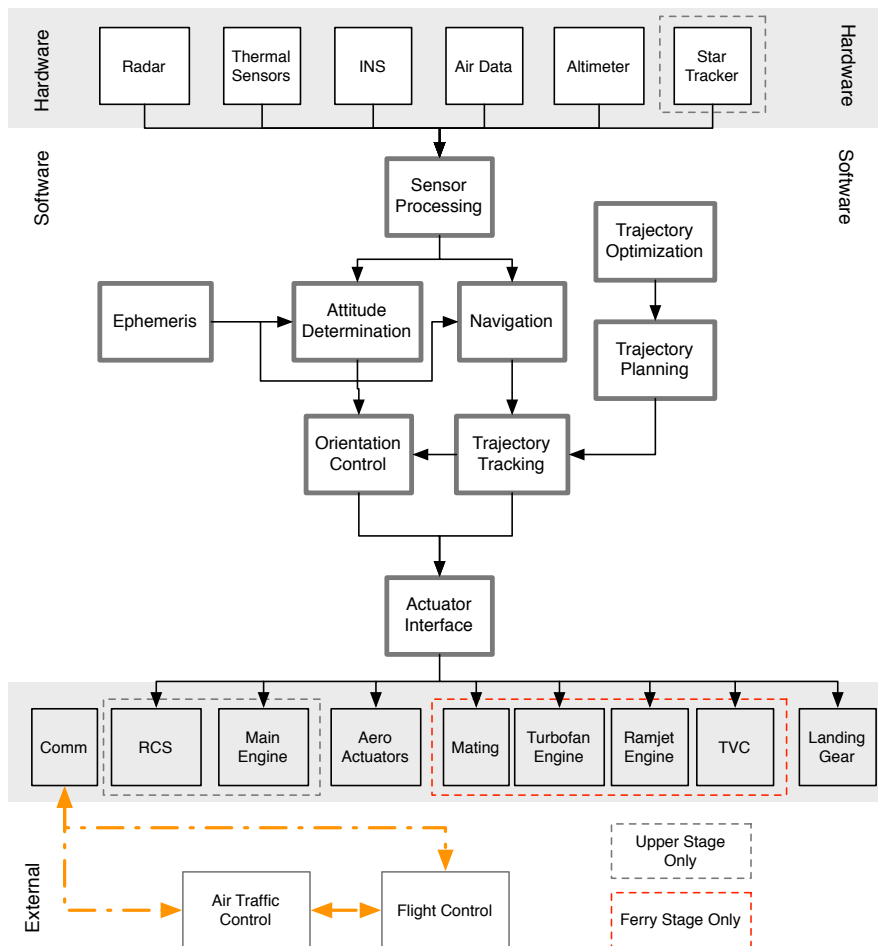

Figure 16: Unified control architecture

6.2 Guidance

The overall design of the guidance and control system for the Integrated Ferry & Orbiter vehicle is illustrated in Figure 17. A pre-computed optimal trajectory provides reference commands for the velocity V_c and flight path angle γ_c over time. The heading command ψ_c is computed based upon the Earth's rotational velocity and the current airspeed V to provide an inertial azimuth angle equal to β, which is given in Eq. 15. The formula for the heading command is:

$$\sin \psi_c = -\left(\frac{V_E}{V}\right)\cos^2 \beta + \cos \beta \sqrt{\tan^2 \beta - \left(\frac{V_E}{V}\right)^2 \sin^2 \beta} \tag{15}$$

where $V_E = R_E \omega_E \cos \theta$ is the rotational velocity of the Earth. The formula shows that if we let $V_E \to 0$, the heading command becomes equivalent to the inertial azimuth angle.

Nonlinear dynamic inversion (NDI) is used to track the desired flight path angle and heading angle using the angle of attack α_c and bank angle ϕ_c. The inner loop control tracks the α_c and ϕ_c commands by commanding the control surface deflections, δ_c. The throttle command σ is determined by comparing the current velocity to the reference velocity. Finally, staging control monitors the velocity, flight path angle, heading, and altitude, and determines when stage separation can occur based on the feasible altitude-velocity envelope of the Orbiter.
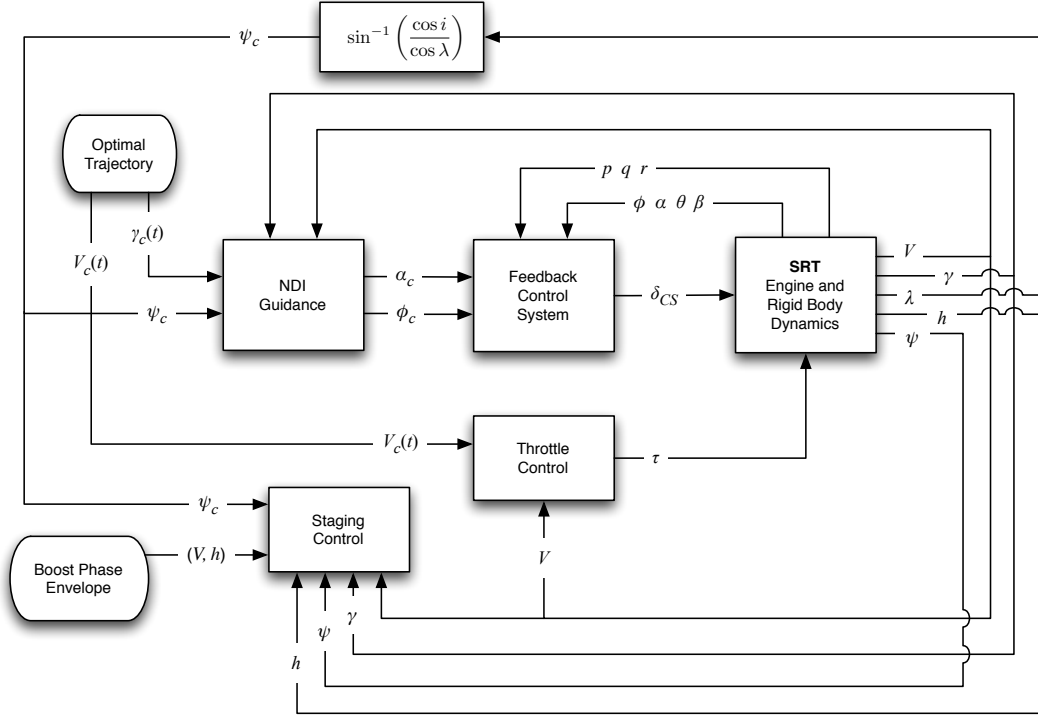

Figure 17: Guidance and Control Framework for Atmospheric Flight

Using the approach of nonlinear dynamic inversion, we first define desired time derivatives for flight path angle and heading:

$$\dot{\gamma}_{Des} = K_\gamma \left(\gamma_c - \gamma \right) \tag{16}$$

$$\dot{\psi}_{Des} = K_\psi \left(\psi_c - \psi \right) \tag{17}$$

where K_γ and K_ψ are control gains that may be gain scheduled to provide desired performance across the flight envelope. Also note that the $\dot{\gamma}_{Des}$ command is limited by the maximum allowable normal acceleration, $n_{\max}$, so that:

$$|\dot{\gamma}_{Des}| \leq \frac{n_{\max}}{V}$$

We now derive the required commands for the angle of attack and bank angle by inverting the dynamic equations. The equations of motion for a point mass aircraft model are:

$$\dot{V} = \frac{1}{m} \left(T - \frac{1}{2} \rho(h) V^2 S C_D(\alpha) \right) \tag{18}$$

$$\dot{\gamma} = \frac{1}{m} \left(\frac{1}{2} \rho(h) V S C_L(\alpha) \right) - \frac{g \cos \gamma}{V} \tag{19}$$

$$\dot{h} = V \sin \gamma \tag{20}$$

$$\dot{\psi} = \frac{\rho(h) V S C_L(\alpha) \sin \phi}{2m \cos \gamma} \tag{21}$$

Using angle of attack to track the flight path angle, we have:

$$\alpha_c = C_L^{-1} \left(\frac{2m \left(\dot{\gamma}_{Des} + g \cos \gamma / V \right)}{\rho(h) V S} \right) \tag{22}$$

where C_L^{-1} represents the inverse function of the lift coefficient. The lift coefficient function will need to be modeled as a function of the angle of attack, altitude, and Mach number. Using bank angle to track the heading, we have:

$$\phi_c = \sin^{-1} \left(\frac{2m \cos \gamma \dot{\psi}_{Des}}{\rho(h) V S C_L(\alpha)} \right) \tag{23}$$

11

6.3 Attitude Control During Separation

Attitude control during separation is done with a combination of aerodynamic surfaces ("flaps") and thrusters. Both translation and attitude must be controlled. The actuator geometry is shown in Figure 18. Two degrees of freedom must be controlled. The flaps can produce positive or negative torques. The thrusters produce unidirectional forces so each produces only a positive or negative torque, not both.
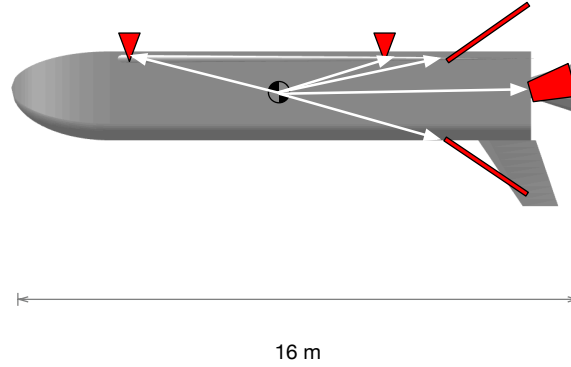

16 m

Figure 18: Orbiter actuator geometry. The red triangles represent thrusters. The red trapezoid indicates the main engine has a gimbal mount. The red line is a flap actuator.

The flaps produce torque due to drag on the plate. Hypersonic drag is highly nonlinear, as shown in Figure 19.
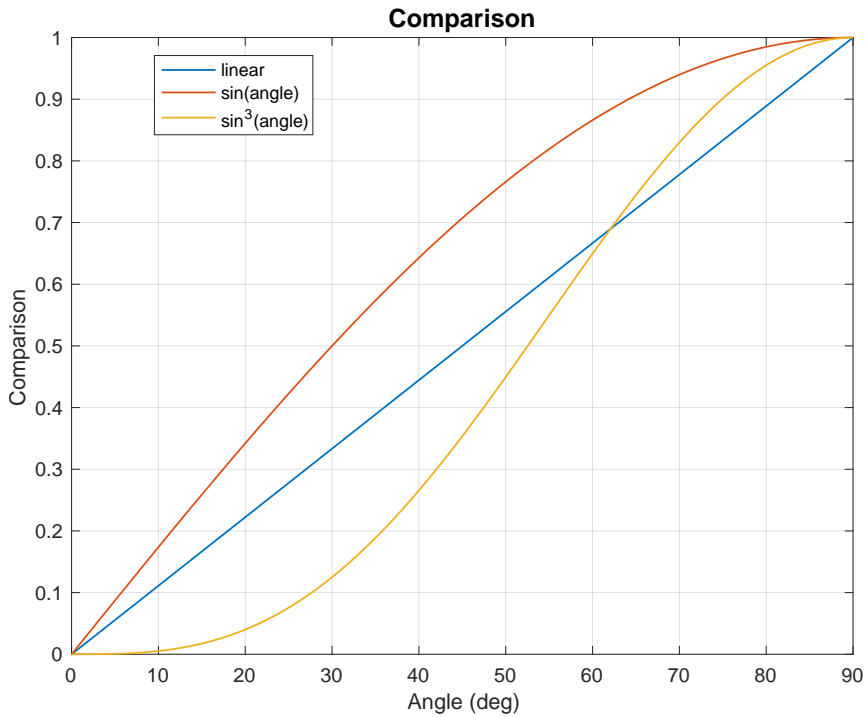
$$D = qC_p \sin^3 \alpha \tag{24}$$

Figure 19: Flap response as a function of angle.

The controller controls the position relative to the target and the orientation during separation and engine ignition. The controller chooses the thruster pulsewidth and flap angle using constrained minimization via the interior-point method. MATLAB's `fmincon` is used, where the cost is the weighted sum of thrust and flap angle. The constraint is the torque demand and is an equality constraint. There are no inequality constraints. The two

thrusters are full-on to produce the separation force and off-pulsed to produce torque. The simulation is at 50 km altitude and Mach 7. Simulation results are shown in Figure 20. Thrusters 1 and 2 are the fore and aft thruster actuators, respectively. The flaps are on the aft side of the vehicle on the top and bottom.
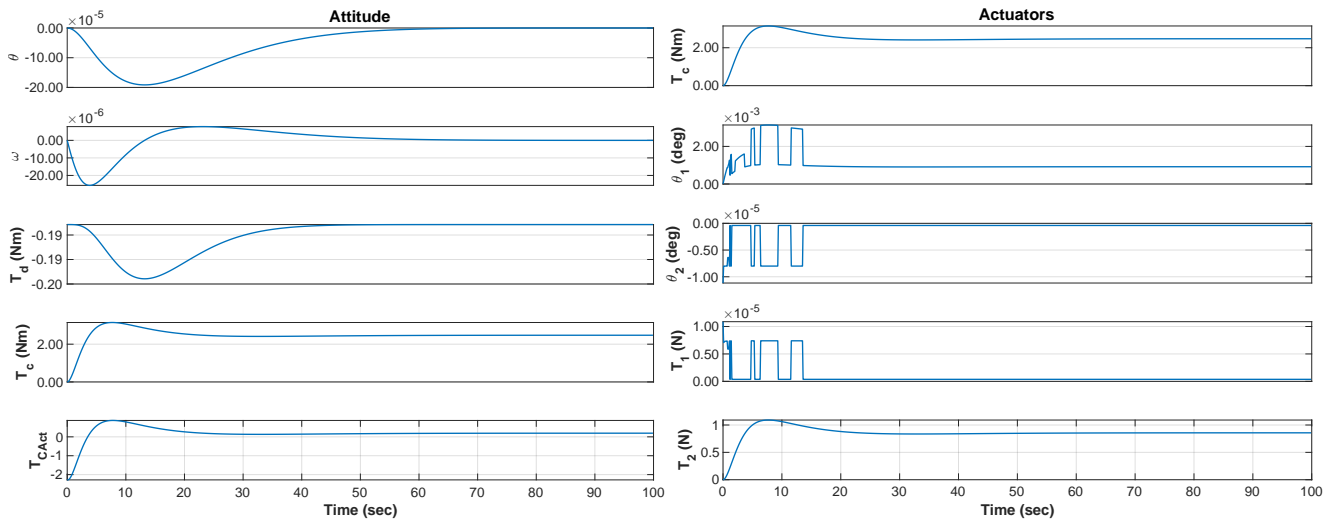

Figure 20: Separation simulation results. Thruster 2 produces most of the control torque.

7. Launch Simulation

Figure 21 shows a typical ascent using the turboramjet. The lefthand plot shows the Ferry stage portion and the full trajectory is on the right. The turboramjet model is ideal so the plots show the best possible performance.
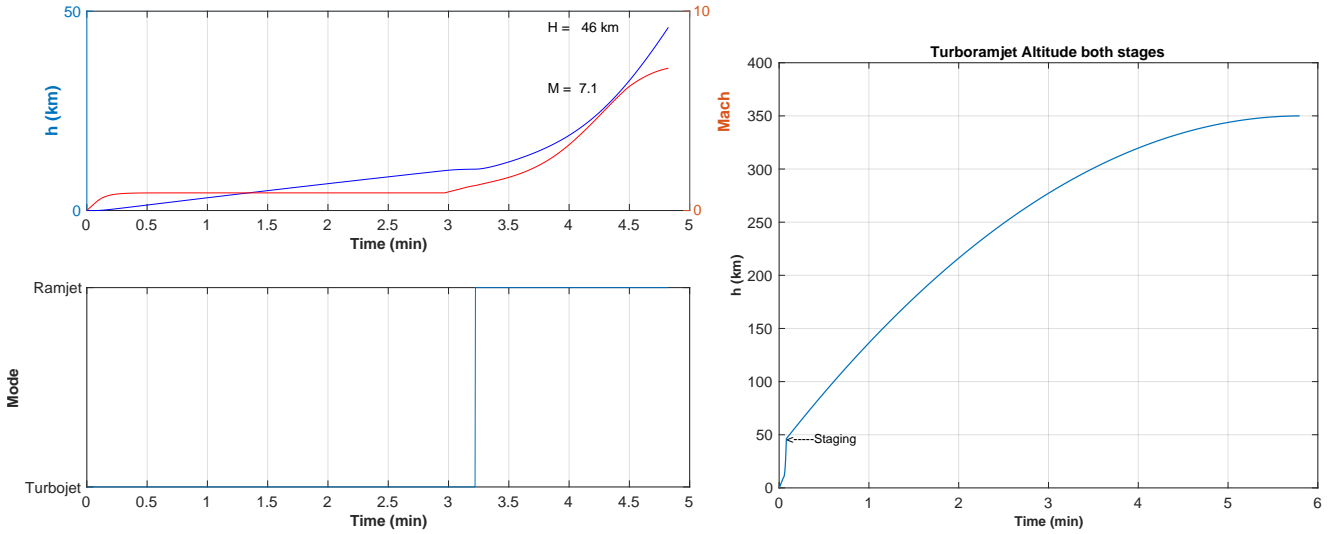

Figure 21: Ascent and full trajectory with the Ferry turboramjet.

Figure 22 shows an ascent using the RDE. The left plot shows the Ferry stage portion and the full trajectory is on the right. The RDE engine follows a shallower trajectory than the turboramjet. The RDE engine model table look-up is limited to Mach 7.5 which is why that is the limit.
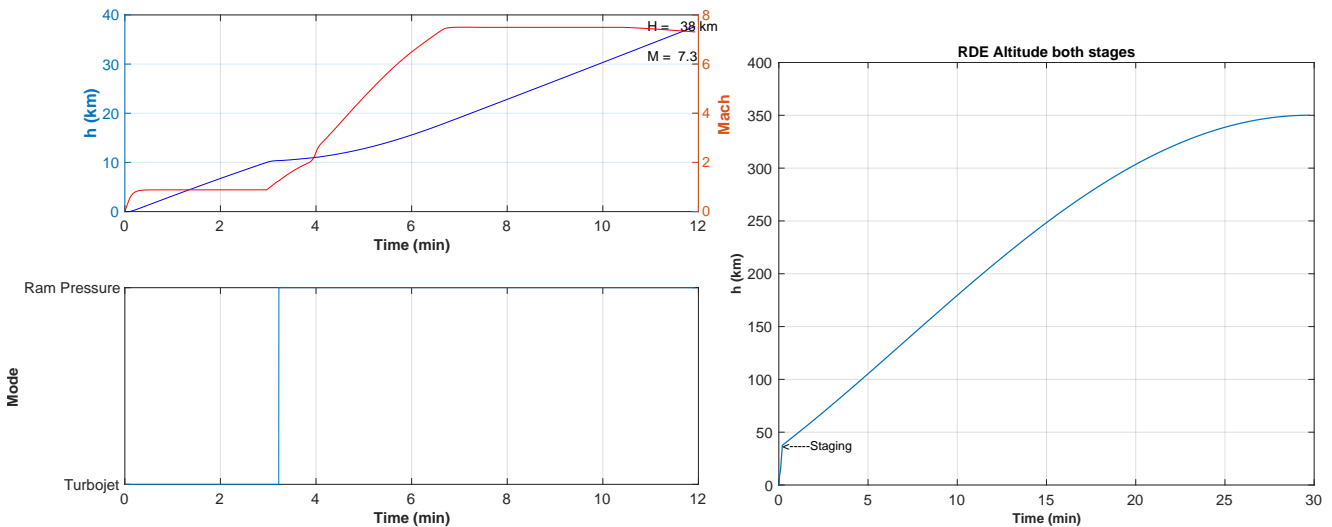

Figure 22: Ascent and full trajectory with the RDE powered Ferry.

8. Trajectory Optimization

The optimal trajectory problem for the Ferry is solved by solving the constrained optimal control problem [33]. The constraint is the end state, which is selected to be the desired Mach number and altitude. We use MATLAB^{TM} function `fmincon` which tries to minimize the costs. `fmincon`, in this case, uses an interior-point algorithm.

The cost is the peak heating rate and fuel consumption. The heat flux is from Equation 10. The optimization is event-based. The approach is to optimize the controller set points. There are two. One is the turbojet set point. The second is the acceleration set point. Both the flight path angle and the Mach number are determined by the optimizer. That gives it four controls. The lower and upper bounds are set to keep the optimizer in plausible regions. The cost is the normalized weighted sum of fuel consumption and heat flux. The constraints are inequality constraints on the altitude and final Mach number.

14

The following listing shows the progress of the optimization. The terms are:

iter Iteration

F-count The number of function calculations

Feasibility Maximum constraint violation

First-order optimality First-order optimality is a measure of how close a point x is to optimal.

Norm ofstep Multiplicative factor that scales the search direction

```
>> OptimalTakeoffFC
                                          First-order       Norm of
 Iter F-count           f(x)   Feasibility  optimality          step
    0       5   7.997503e+09    1.206e+02   3.480e+11
    1      10   7.752072e+09    0.000e+00   3.513e+11    1.493e-01
    2      15   7.260326e+09    4.816e-05   1.361e+11    2.269e-02
    3      20   6.952523e+09    0.000e+00   7.993e+09    3.232e-02
    4      25   5.323442e+09    0.000e+00   8.986e+09    2.010e-01
    5      30   4.327589e+09    2.339e+02   1.442e+11    1.134e-01
    6      35   4.366311e+09    2.935e+02   4.239e+10    3.020e-02
    7      40   4.539524e+09    3.707e+02   4.490e+10    1.307e-02
    8      45   4.540140e+09    3.714e+02   6.206e+09    4.374e-06
    9      50   4.540143e+09    3.714e+02   1.118e+09    7.554e-08
   10      55   4.540102e+09    3.713e+02   1.100e+09    3.437e-05
   11      64   4.236357e+09    3.312e-01   8.592e+09    1.071e-03
   12      69   4.239383e+09    3.290e-01   8.577e+09    1.605e-02
   13      74   4.239398e+09    3.289e-01   7.441e+09    8.451e-07
   14      79   4.239421e+09    3.289e-01   7.438e+09    1.014e-03
   15      87   4.239714e+09    3.287e-01   7.427e+09    9.200e-03
   16      96   4.239419e+09    3.289e-01   7.313e+09    1.798e-04
   17     101   4.239419e+09    3.289e-01   7.313e+09    1.669e-03
   18     106   4.239826e+09    3.287e-01   7.322e+09    9.385e-02
   19     111   4.240040e+09    3.285e-01   7.314e+09    1.262e-01
   20     118   4.240216e+09    3.284e-01   7.308e+09    1.919e-04
   21     130   4.240304e+09    3.284e-01   2.790e+07    4.764e-05
   22     135   4.240327e+09    3.283e-01   2.790e+07    4.743e-04
   23     149   4.240360e+09    3.283e-01   2.500e+07    2.008e-05
   24     161   4.240362e+09    3.283e-01   2.491e+07    1.169e-06
   25     172   4.240363e+09    3.283e-01   5.000e-01    1.283e-07

Optimization stopped because the relative changes in all elements of x are
less than options.StepTolerance = 1.000000e-10, but the relative maximum
    constraint
violation, 2.722480e-03, exceeds options.ConstraintTolerance = 1.000000e-06.
```

Figure 23 shows the starting trajectory. Figure 24 shows the optimal trajectory. The controls are the Mach number and flight path angle in turbojet mode and acceleration mode. The control system takes those set points and uses angle of attack and throttle setting to achieve the set points. The optimal trajectory limits the Mach number slightly to reduce the heating load.

9. DEVELOPMENT

Horizontal takeoff launch vehicles have been studied since the 1950's. The advent of reusable first stages, such as on the SpaceX Falcon-9, has helped lower the cost of vertical launch. Horizontal takeoff requires the development of the first-stage engine, and possibly a new second-stage engine. Figure 25 shows a development plan for SRT. SRT provides a unique development path. Both vehicles share the same GN&C system so that work can be done in parallel. The Orbiter could be launched on any booster for testing, much like the X-37B is today. It would only require a first stage for orbital operations. The Orbiter, by itself, is a viable second stage for any launch vehicle. The development timeline is similar to that of the F-35 fighter. The exact dates would depend on the level of funding. The Ferry engine is the most challenging part of the development. One mitigating factor is that it is an accelerator and does not require operation during sustained cruise flight. This somewhat reduces the material challenges.

The development cost of the Ferry engine is a key consideration. The RAND Corporation studied military engine procurement [34]. Using their model, which is a function of inlet temperature, the cost for developing the
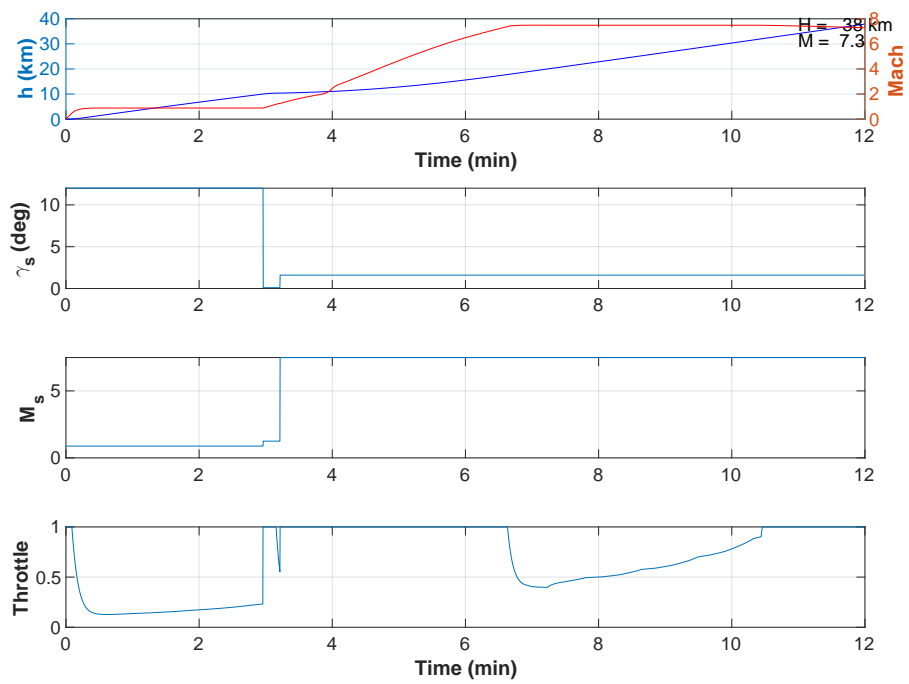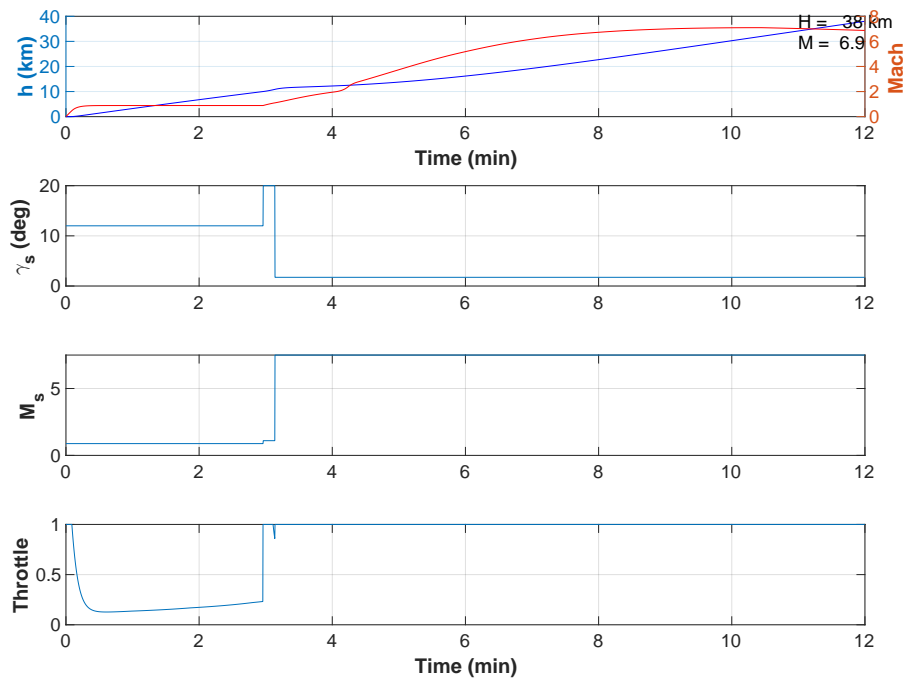
Figure 23: Ferry starting trajectory.

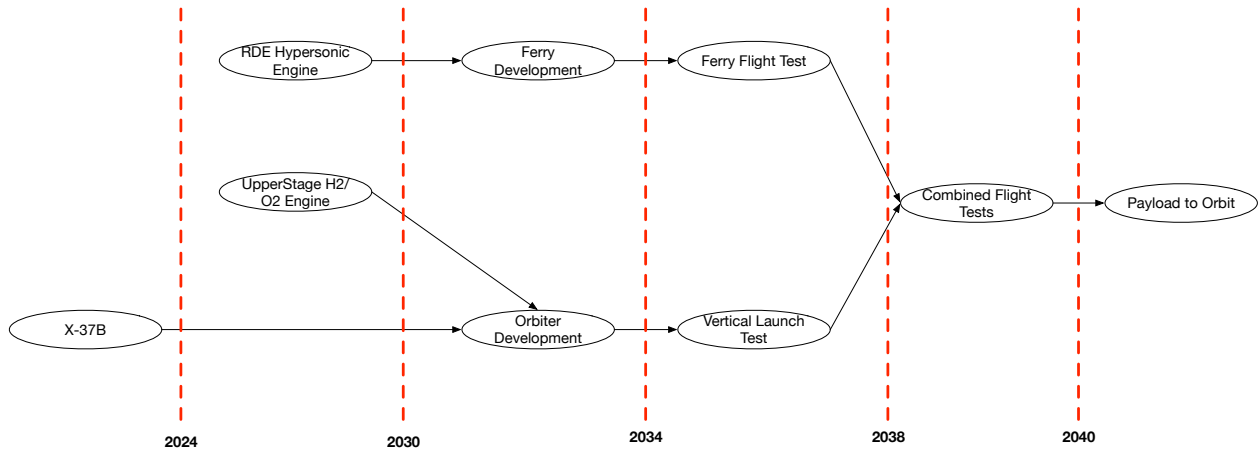**Figure 24:** Ferry optimal trajectory.

Figure 25: SRT provides a unique low-risk development path.

proposed first-stage engine would be $12B USD in 2024 dollars assuming the inlet temperature is the stagnation temperature at 40 km at Mach 7. In comparison, the U.S. has spent over $50B USD on the Space Launch System and the Orion spacecraft. Given the benefits of this new engine, the cost is not unreasonable.

10. Conclusions

This paper analyzes a two-stage to-orbit launch vehicle using an RDE ramjet. The trajectory optimization includes weighting the thermal stress on the engine. Future work will be detailed CFD studies of the configuration and end-to-end trajectory optimization using CFD-based models. Further work on RDE combustion stability is needed. More sophisticated RDE engine models are needed to verify the performance. The inlet and nozzle need to be studied for the Ferry stage. A variable geometry nozzle will be needed to optimize the flight performance. The masses of both stages need to be refined. Currently, they are based on mass models that are not specifically designed for hypersonic vehicles.

11. Acknowledgements

References

[1] Mueller, J. B. and Paluszek, M. A., "Space Rapid Transit - A Two Stage to Orbit Fully Reusable Launch Vehicle," *International Astronautical Congress*, No. IAC-14,C4,6.2, October 2014.

[2] Mueller, J. B., Griesemer, P. R., Paluszek, M. A., and Du, J., "Unified GN&C System for the Space Rapid Transit Launch Vehicle," *AIAA GN&C Conference*, August 2010.

[3] Griesemer, P., Mueller, J., Paluszek, M., and Du, J., "System Design of a Reusable, Horizontal Take-Off/Horizontal Landing Two Stage to Orbit Vehicle," *Joint Propulsion Conference*, Nashville, TN, July 2010.

[4] Griesemer, P., Mueller, J., Paluszek, M., and Raghavan, P., "Space Rapid Transit Navigation and Control," *EUCASS 2011*, St. Petersburg Russia, July 2011.

[5] Griesemer, P., Mueller, J., Paluszek, M., and de Castro, E., "Space Rapid Transit for Rapid Spacecraft Deployment," *2011 Reinventing Space Conference*, Los Angeles, California, July 2011.

[6] Flight Global, "Sänger Aerospace Plane Gains Momentum," http://www.flightglobal.com/pdfarchive/view/1989/1989%20-%202466.html.

[7] Limited, R. E., "Reaction Engines Limited," http://www.reactionengines.co.uk/index.html.

[8] Beil, A., "Chinese spaceplane takes flight again; iSpace and LandSpace prepare to hop," *NSF*, December 2023.

[9] Roulette, J. and Gorman, S., "US military's secretive spaceplane launched on possible higher-orbit mission," *Reuters*, December 2023.

[10] Jones, A., "China launches mystery reusable spaceplane for third time," December 2023, https://spacenews.com/china-launches-mystery-reusable-spaceplane-for-third-time/.

[11] Garofalo, M., "Sierra Space unveils Dream Chaser space plane ahead of 1st flight to ISS (video)," *Space.com*, February 2024, https://www.space.com/sierra-space-unveils-dream-chaser-space-plane-photos.

[12] LIN, J. and SINGER, P., "China's Hybrid Spaceplane Could Reset The 21st Century Space Race," *Popular Science*, August 2016.

[13] Kingbury, N., "Aerospace Plane Technology Research and Development in Europe," Tech. Rep. GAO/NSIAD-91-194, GAO, August 1992.

[14] van Pelt, M., *Rocketing into the Future The History and Technology of Rocket Planes*, Springer, 2012.

[15] Trimble, S., "Rotating Detonation Sparks GE Path To Hypersonic Future," *Aviation Week*, December 2023.

[16] GE, "GE Aerospace Demonstrates Hypersonic Dual-Mode Ramjet with Rotating Detonation Combustion," December 2023.

[17] Wolfe, F., "Hermeus Tests Turbine-Based Cycle Engine for Reusable Hypersonic Aircraft," *Defense Daily*, November 2022.

[18] Burkardt, L. and Norris, R., "The design and evolution of the Beta two-stage-to-orbit horizontal takeoff and landing launch system," *AIAA 4th International Aerospace Planes Conference, Orlando FL*, 1992.

[19] Varvill, R. and Bond, A., "The SKYLON Spaceplane," *JBIS*, Vol. 57, 2004, pp. 22–32.

[20] Baldwin, B., *Pegasus User's Guide Release 7.0*, Orbital Sciences Corporation, April 2010.

[21] "http://www.virgingalactic.com/launcherOne/," 2014.

[22] Wolanski, P., "Detonation engines," *Journal of KONES Powertrain and Transport*, Vol. 18, 01 2011, pp. 515–521.

[23] Threewitt, C., "How the Rotating Detonation Engine Works," July 2013.

[24] Goto, K., Matsuoka, K., Matsuyama, K., Kawasaki, A., Watanabe, H., Itouyama, N., Ishihara, K., Buyakofu, V., Noda, T., and Kasahara, J., "Flight Demonstration of Detonation Engine System Using Sounding Rocket S-520-3: Performance of Rotating Detonation Engine," *AIAA SCITECH 2022 Forum*, January 2022.

[25] Institute of Materials and Systems for Sustainability (IMaSS), "World First! Successful Space Flight Demonstration of Detonation Engines for Deep Space Exploration," https://www.imass.nagoya-u.ac.jp/en/research/20210819__kasahara.html.

[26] Law, H., Baxter, T., Ryan, C., and Deiterding, R., "Design and testing of a small-scale laboratory rotating detonation engine running on ethylene-oxygen," *AIAA Propulsion and Energy 2021 Forum*, August 2021.

[27] Anand, V. and Gutmark, E., "Rotating detonation combustors and their similarities to rocket instabilities," *Progress in Energy and Combustion Science*, Vol. 73, 2019, pp. 182–234.

[28] HOLLINGS, A., "GE'S HYPERSONIC ROTATING DETONATION ENGINE BREAKTHROUGH COULD CHANGE AVIATION FOREVER," *SANDBOXX*, January 2024.

[29] Paluszek, M., Galea, C., Simpkins, M., Ju, Y., and Shneider, M., "Rotating Detonation Engine for Hypersonic Flight," *HiSST 2022*, September 2022.

[30] Shepherd, J. E., "Shock and Detonation Toolbox - 2018 Version," .

[31] Goodwin, D. G., Moffat, H. K., Schoegl, I., Speth, R. L., and Weber, B. W., "Cantera: An Object-oriented Software Toolkit for Chemical Kinetics, Thermodynamics, and Transport Processes," https://www.cantera.org, 2023, Version 3.0.0.

[32] Sook-Ying, H. and Paull, A., "Coupled thermal, structural and vibrational analysis of a hypersonic engine for flight test," Jul 2006.

[33] Paluszek, M., Thomas, S., and Ham, E., *Practical MATLAB Deep Learning*, Apress, 2022.

[34] Younossi, O., Arena, M. V., Moore, R. M., Lorell, M. A., Mason, J., and Graser, J. C., *Military Jet Engine Acquisition: Technology Basics and Cost-Estimating Methodology*, RAND Corporation, Santa Monica, CA, 2003.